

## Molecular Dynamics Simulations of the d(CCAACGTTGG)<sub>2</sub> Decamer: Influence of the Crystal Environment

David R. Bevan,\* Leping Li,<sup>†</sup> Lee G. Pedersen,<sup>†</sup> and Thomas A. Darden<sup>†</sup>

\*Department of Biochemistry, Virginia Polytechnic Institute and State University, Blacksburg, Virginia 24061, and <sup>†</sup>Laboratory of Structural Biology, National Institute of Environmental Health Science, Research Triangle Park, North Carolina 27709 USA

**ABSTRACT** Molecular dynamics (MD) simulations of the DNA duplex d(CCAACGTTGG)<sub>2</sub> were used to study the relationship between DNA sequence and structure. Two crystal simulations were carried out; one consisted of one unit cell containing two duplexes, and the other of two unit cells containing four duplexes. Two solution simulations were also carried out, one starting from canonical B-DNA and the other starting from the crystal structure. For many helicoidal parameters, the results from the crystal and solution simulations were essentially identical. However, for other parameters, in particular,  $\alpha$ ,  $\gamma$ ,  $\delta$ ,  $(\epsilon - \zeta)$ , phase, and helical twist, differences between crystal and solution simulations were apparent. Notably, during crystal simulations, values of helical twist remained comparable to those in the crystal structure, to include the sequence-dependent differences among base steps, in which values ranged from 20° to 50° per base step. However, in the solution simulations, not only did the average values of helical twist decrease to ~30° per base step, but every base step was ~30°, suggesting that the sequence-dependent information may be lost. This study reveals that MD simulations of the crystal environment complement solution simulations in validating the applicability of MD to the analysis of DNA structure.

### INTRODUCTION

Understanding factors associated with essential cellular processes such as replication and transcription will lead to an enhanced ability to regulate these processes and thereby treat a variety of diseases more effectively. Of importance in replication and transcription are the structure and dynamics of DNA, which are dependent to some extent on DNA sequence (Hunter, 1996). Thus an improved understanding of the relationship between DNA sequence and structure is a subject of considerable interest.

Methods that may be used to examine the relationship between DNA sequence and structure include x-ray crystallography, NMR, and theoretical methods such as molecular dynamics (MD). X-ray crystallography has proved to be particularly valuable in the examination of DNA structure, but the principal limitation of this technique is the need to obtain high-quality crystals for every sequence of interest. Another criticism that is sometimes invoked is that crystal packing effects may constrain the DNA structure, thereby confounding an analysis of the relationship of sequence to structure (Ramakrishnan and Sundaralingam, 1993; Tippin and Sundaralingam, 1997). NMR has also proved valuable in the structural analysis of DNA, but a problem associated with NMR is that the data are relatively short-ranged, and consequently fewer data can be collected when an extended structure like DNA is studied, as compared to more globular structures like proteins (Hartmann and Lavery, 1996). As a result, NMR structures of DNA, in the absence of dipolar

anisotropic coupling data, tend to be of a lower resolution than crystal structures. Theoretical approaches such as MD are being applied more frequently in studies of DNA structure, especially since the application of Ewald methods to electrostatics has led to better agreement between simulation and experiment (Darden et al., 1999; York et al., 1993, 1994, 1995). However, MD is still not sufficiently tested to be used routinely to study sequence-dependent structural differences in DNA. Nevertheless, it is important to extend the applicability of MD because it can provide an atomic-level description of DNA structure and dynamics that will prove valuable for interpreting experimental data and developing models of DNA structure and function.

Recent review articles highlight various aspects of MD simulations of nucleic acids (Cheatham et al., 1998; Jayaram and Beveridge, 1996; Westhof et al., 1995). Several recent papers describe results that are pertinent to our studies and that exemplify the current state of MD simulations of nucleic acids. For example, Cheatham and Kollman (1996) performed MD on DNA duplexes of the sequence d(CCAACGTTGG)<sub>2</sub>, as we have done. They carried out four MD simulations, two starting from canonical B-DNA and two from canonical A-DNA. All simulations produced structures with characteristics of B-DNA that were within 0.8–1.6 Å root mean square (RMS) deviation of one another and 3.1–3.6 Å RMS deviation of the published crystal structure (Prive et al., 1991). During the MD simulation starting from canonical A-DNA, a transition to B-DNA was observed on a nanosecond time scale, indicating that the energy barrier for transition from A- to B-DNA was not prohibitive. Other recent studies include MD simulations of the dodecamer d(CGCGAATTCGCG)<sub>2</sub>. This structure has been studied extensively because it was the first duplex to be crystallized and because it contains the recognition site of the *EcoRI* restriction enzyme. In one of the studies, Duan

Received for publication 7 June 1999 and in final form 8 October 1999.

Address reprint requests to Dr. David R. Bevan, Department of Biochemistry, 201 Fralin Biotechnology Center, Virginia Tech, Blacksburg, VA 24061-0308. Tel: 540-231-5040; Fax: 540-231-9070; E-mail: drbevan@vt.edu.

© 2000 by the Biophysical Society

0006-3495/00/02/668/15 \$2.00



et al. (1997) ran simulations starting from the crystal structure of the duplex as it exists in a complex with the endonuclease. In this complex the duplex is kinked. MD simulation produced a structure that was no longer kinked and was closer, based on RMS deviation, to the crystal structure of the duplex in the absence of the protein. These investigators also noted some evidence of sequence-dependent structural features and a spine of hydration in the minor groove. Beveridge and co-workers have carried out extensive MD simulations on nucleic acids, including two very recent studies on the  $d(\text{CGCGAATTCGCG})_2$  dodecamer (Young et al., 1997a,b). The starting structure for these studies was canonical B-DNA. Several simulations were carried out to examine the effects of initial counterion placement and the method of calculating electrostatic interactions (i.e., truncated potentials versus particle mesh Ewald). One of the significant findings of these studies was that  $\text{Na}^+$  counterions may enter the spine of hydration in the minor groove of DNA, possibly in a sequence-specific manner. This observation extends hypotheses that water molecules that constitute the spine of hydration may stabilize DNA structure.

An impressive aspect of the simulations cited above is that structural features characteristic of B-DNA are maintained over several nanoseconds. However, not all features are preserved (e.g., helical twist), so it is necessary to reconcile the results from simulation with those from experimental methods such as crystallography. An additional approach that can be applied in MD is simulations that start from the crystal structure, with the crystal environment maintained throughout the simulation (crystal simulation). Differences that arise between crystal structure and simulated structure may facilitate the identification of force-field parameters that need to be adjusted to improve agreement between experiment and simulation. Some crystal simulations of nucleic acids have been reported. For example, Darden and co-workers performed a series of crystal simulations when they were demonstrating the efficacy of the Ewald methods. An MD simulation of the dodecamer  $d(\text{CGCGAATTCGCG})_2$  in the crystal unit cell yielded a stable trajectory and an average structure with an RMS deviation for all heavy atoms of 1.16 Å from the crystal structure (York et al., 1995). Similarly, an MD simulation of Z-DNA ( $d[\text{CGCGCG}]_2$ ) in its crystal environment produced an average structure with an RMS deviation of 0.5 Å from the crystal structure (Lee et al., 1995b). MD simulations of the RNA dinucleotides ApU and GpC were also undertaken (Lee et al., 1995a). These molecules represent a particular challenge for MD because all heavy atom positions in the crystal are known, to include nucleotide, counterion, and water positions. The average structures from MD simulations of the dinucleotides were within 0.4 Å of the crystal structures, and the calculated and experimental temperature factors were comparable. These results suggest that crystal simulations may provide a means of performing MD sim-

ulations under conditions in which many structural features of nucleic acids are preserved without the molecules being overly constrained within the crystal lattice. Moreover, a direct comparison between crystal structure and crystal simulation provides a way to rigorously evaluate the quality of the simulations.

As noted above, crystal packing effects are sometimes cited as a limitation of crystallography in the analysis of DNA structure. Dickerson has effectively argued that crystal packing may constrain the DNA conformation in the crystal, but the DNA can only adopt structures that are favored by its sequence (Dickerson et al., 1994). That is, crystal packing does not force the DNA into structures that it could not otherwise assume. It also bears mentioning that analysis of structures in solution, whether by NMR or MD, also may not represent a realistic environment for the state of DNA in cells. In the nucleus, where the density is 1.3–1.4 g/ml (Sheeler and Bianchi, 1980), DNA is tightly packed and constrained in a manner that may be more similar to its crystalline than to its solution state.

In the studies described here, we report MD simulations of the DNA decamer  $d(\text{CCAACGTTGG})_2$  in the crystal environment. A simulation including one unit cell containing two duplexes was run for 25 ns, and a simulation including two unit cells containing four duplexes was run for 15 ns. We also conducted solution simulations for comparison. These long simulations enabled us to examine in detail the stability of the duplexes during the simulations.

## METHODS

### General methods

Four MD simulations were conducted as part of this project. Two of them were simulations of the crystal environment, one involving a single unit cell containing two DNA duplexes, and the other two unit cells containing four duplexes. The other two simulations were solution simulations in which a single duplex was immersed in a box of water. For one of the solution simulations the starting structure was canonical B-DNA, and for the other the starting structure was the crystal structure. Structures were visualized using Visual Molecular Dynamics (VMD) (Humphrey et al., 1996). All modeling was done with AMBER4.1 programs (Pearlman et al., 1995) implemented on Silicon Graphics computers with R10000 processors. The Cornell et al. (1995) force field was used. MD simulations were conducted with the SANDER module of AMBER. Simulations were carried out with a 2-fs time step at 300 K. The SHAKE algorithm was applied to all bonds involving hydrogen atoms. Van der Waals interactions were calculated using an 8-Å atom-based nonbond list, while the long-range Coulomb energy was evaluated by the particle-mesh-Ewald (PME) method (Essmann et al., 1995). Specific details pertaining to each simulation are given below.

## Crystal simulations

### One unit cell

The starting coordinates for the crystal simulations were taken from the PDB file with code 5dnb (Prive et al., 1991). The PDB file contains coordinates for only one strand of the duplex, so the remaining strand was generated through the appropriate symmetry transformation. A second duplex was added to the unit cell by translating the initial duplex according to guidelines published by Prive et al. (1991). An illustration of the arrangement of the two duplexes is given in Fig. 1. The crystallographic positions of the  $Mg^{2+}$  ions were maintained during the generation of the unit cell, with 14  $Mg^{2+}$  ions present in the system. Crystallographic waters were added by applying the appropriate symmetry transformations, as was done to generate the duplex structures, and then by adding hydrogen atoms, using the GWH utility within AMBER. The EDIT and PARM modules of AMBER were then used to generate topology and coordinate

files containing positions of DNA atoms,  $Mg^{2+}$  ions, and crystallographic water molecules. Bulk water molecules were then added to the system, and minimization was carried out to adjust the positions of water molecules that were in close contact with other atoms in the system. To achieve electroneutrality, eight bulk water molecules were selected randomly and converted into  $Na^+$  ions. The energy of the system was then minimized to remove bad atom-atom contacts. After minimization, MD was run for 100 ps, during which the DNA,  $Mg^{2+}$  ion, and crystallographic water positions were fixed and the bulk water molecules and  $Na^+$  ions were allowed to move. We then attempted to perform MD with decreasing constraints on the crystallographic waters, but we encountered unrealistically high energies. This problem was traced to the wrapping option in the SANDER module of AMBER. That is, water molecules that were wrapped to an adjacent periodic box were being constrained to a position in the original box, thereby generating large constraint energies. Thus wrapping was turned off for

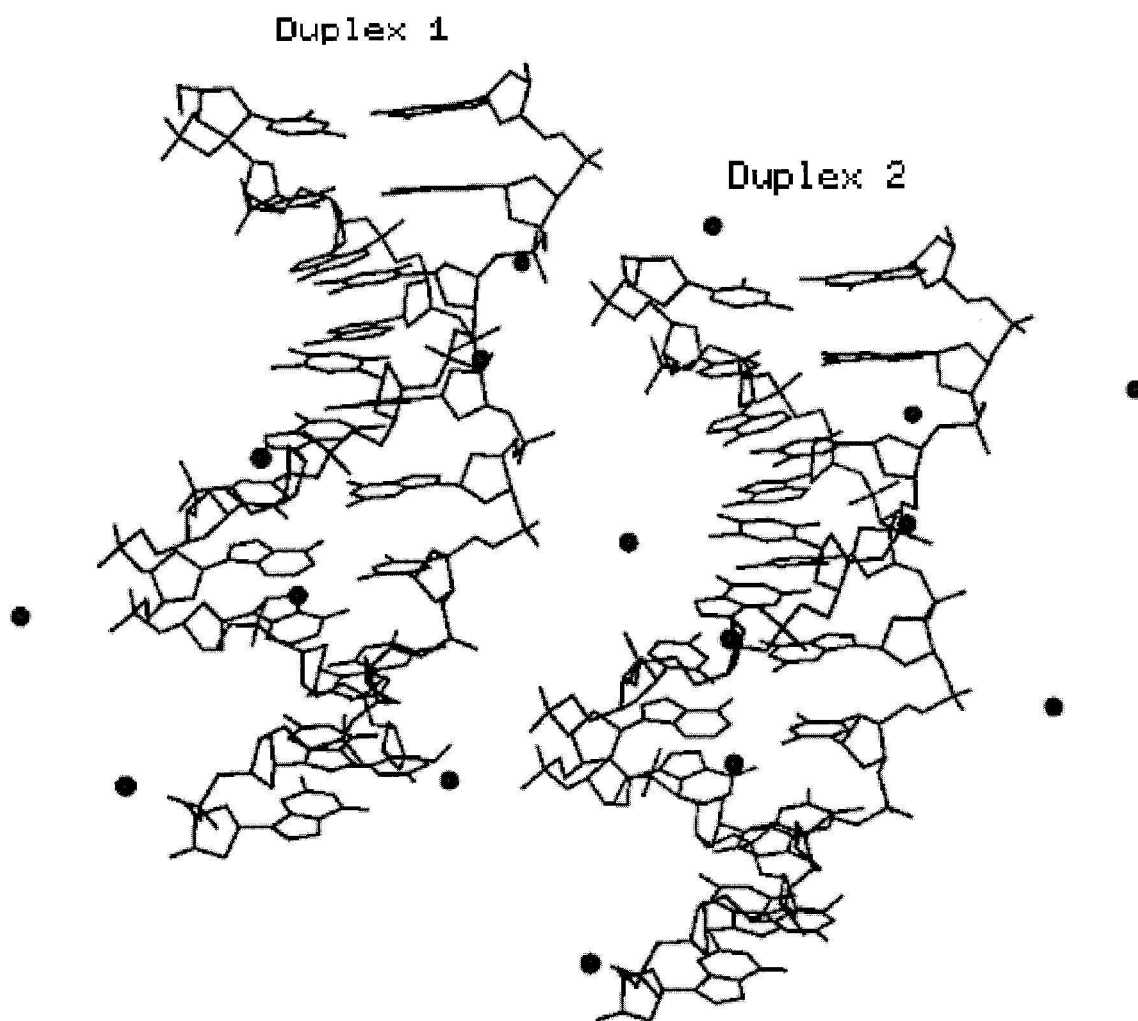


FIGURE 1 The arrangement of the two duplexes in the unit cell. The circles represent the positions of the  $Mg^{2+}$  ions.



subsequent MD simulations, which would have no effect on forces and energies but was done for convenience of analysis. MD was then carried out at 300 K, during which bulk water molecules and Na<sup>+</sup> ions were allowed to move, but crystallographic waters were constrained so that they did not move a significant distance from their crystallographic positions. The system was then minimized, first by minimizing bulk waters and Na<sup>+</sup> ions; then bulk waters, Na<sup>+</sup> ions, and crystal waters; then all hydrogen atoms; and finally the complete system.

At this point, we determined if additional water molecules were needed in the system to model the crystal environment. That is, we needed to maintain constant volume and density during MD simulations. The minimized system was heated from 0 to 300 K over a period of 30 ps and then equilibrated for an additional 50 ps, all at constant volume. A 50-ps MD simulation at constant pressure was then conducted. The box decreased in volume and increased in density during the MD, indicating that additional water molecules were needed. Water molecules were added by determining where in the unit cell they could be added without being in close contact with other atoms. Several cycles of water packing, followed by minimization and MD as described above, were necessary to generate a unit cell in which the volume and density were stable during MD. The density in this system, which contained 2882 atoms, was 1.4 g/ml. This system was then minimized and used for the extended MD simulation. MD was begun by heating from 0 to 300 K over 30 ps and then running under constant volume conditions for 1 ns. Constant pressure conditions were then imposed, and the MD was continued for a total simulation time of 25 ns.

#### *Two unit cells*

A system consisting of two unit cells was constructed by translating a copy of the original unit cell in the Z-dimension (Prive et al., 1991), giving a system of 5764 atoms. This simulation enabled us to increase the amount of sampling during a single simulation and to determine if the results were altered by relieving the end-to-end constraints imposed by periodic boundary conditions. MD was run by heating the system from 0 to 300 K over 30 ps, running constant-volume MD for an additional 50 ps, and then running constant-pressure MD for a total simulation time of 15 ns.

### **Solution simulations**

#### *Canonical B-DNA*

This solution simulation was based on methods described by Cheatham and Kollman (1996). Canonical B-DNA was built using the NUCGEN module of AMBER. Na<sup>+</sup> counterions and water were added in LEAP. The size of this

system was 9440 atoms. The system was equilibrated by running MD for 80 ps at 500 K and then for 20 ps at 300 K. The system was then subjected to energy minimization, first with the DNA atoms fixed and then with no constraints. After minimization, the system was heated first by running MD for 10 ps at 100 K, then for 10 ps at 200 K, and finally for 23 ps at 300 K, with all of these steps at constant volume. Constant pressure conditions were then imposed for the remainder of the simulation, which proceeded for a total of 12 ns.

#### *Crystal structure*

The crystal coordinates from PDB file 5dnb were used for the DNA structure. The crystallographic counterions and water molecules were not used. Na<sup>+</sup> counterions and water were added in LEAP, giving a system of 9083 atoms. The system was equilibrated by running MD for 100 ps while the DNA atom positions were fixed. The system was then minimized, by minimizing water and Na<sup>+</sup> ions and then all atoms. The system was heated from 0 to 300 K over a period of 30 ps under constant-volume conditions. It was further equilibrated for 50 ps at constant volume, after which constant pressure was imposed for the remainder of the simulation, which was run for 5 ns.

### **Data analysis**

Coordinates for analysis were saved every picosecond during the simulations. DNA structural parameters were calculated with Curves 5.1 (Lavery and Sklenar, 1988). A global helical analysis was used in the Curves analysis. Except where noted, structural parameters for the various simulations were obtained by averaging over the following time periods: one unit cell crystal simulation, 20–25 ns; two unit cell crystal simulation, 10–15 ns; solution simulation starting from canonical B-DNA, 10–12 ns; solution simulation starting from the crystal structure, 4–5 ns. Average values for helicoidal parameters were obtained by averaging the values for the individual structures collected at 1-ps intervals over the time periods indicated.

## **RESULTS**

### **Analysis of DNA structure**

Many of the data pertaining to DNA structure from the simulations are summarized in Table 1. Results from the one unit cell simulation will be discussed first, followed by the results from the two unit cell simulation, after which a comparison of these crystal simulations with the solution simulations will be made.

#### *One unit cell simulation*

Shown in Fig. 2 is the RMS deviation, relative to the starting structure, for the two duplexes in the one unit cell



**TABLE 1** Helicoidal parameters for the duplexes from the crystal structure and the molecular dynamics simulations

Parameter	5dnb	One-1	One-2	Two-1	Two-2	Two-3	Two-4	Solution (canonical)	Solution (crystal)
$\alpha$ (deg)	296.6	262.9 $\pm$ 2.9	255.4 $\pm$ 2.5	275.9 $\pm$ 3.0	269.2 $\pm$ 2.7	265.5 $\pm$ 3.5	255.2 $\pm$ 5.5	285.8 $\pm$ 4.7	291.1 $\pm$ 2.5
$\beta$ (deg)	166.3	169.6 $\pm$ 3.1	172.7 $\pm$ 2.6	165.9 $\pm$ 2.7	172.6 $\pm$ 3.1	169.9 $\pm$ 2.9	164.2 $\pm$ 3.1	167.8 $\pm$ 4.1	171.8 $\pm$ 2.4
$\gamma$ (deg)	49.2	76.9 $\pm$ 3.3	85.9 $\pm$ 3.0	68.9 $\pm$ 4.7	75.9 $\pm$ 4.7	77.6 $\pm$ 3.6	89.8 $\pm$ 3.6	69.3 $\pm$ 4.3	69.0 $\pm$ 2.8
$\delta$ (deg)	128.7	135.4 $\pm$ 2.2	131.4 $\pm$ 2.3	131.6 $\pm$ 3.1	130.0 $\pm$ 3.2	135.5 $\pm$ 2.7	135.1 $\pm$ 2.5	115.1 $\pm$ 4.0	111.7 $\pm$ 4.2
$\epsilon$ (deg)	204.9	225.5 $\pm$ 3.1	215.0 $\pm$ 3.3	217.9 $\pm$ 5.0	205.8 $\pm$ 6.0	216.7 $\pm$ 3.9	218.7 $\pm$ 3.5	194.3 $\pm$ 3.7	189.9 $\pm$ 3.3
$\zeta$ (deg)	239.7	229.8 $\pm$ 3.0	238.9 $\pm$ 3.3	238.7 $\pm$ 5.6	249.6 $\pm$ 6.3	229.9 $\pm$ 4.4	238.7 $\pm$ 3.7	266.6 $\pm$ 4.3	270.9 $\pm$ 3.9
$\chi$ (deg)	257.7	254.4 $\pm$ 2.7	250.8 $\pm$ 3.0	252.7 $\pm$ 3.6	246.0 $\pm$ 3.8	260.5 $\pm$ 3.2	253.1 $\pm$ 2.8	231.5 $\pm$ 3.9	229.5 $\pm$ 4.4
Phase (deg)	145.5	150.5 $\pm$ 3.8	145.0 $\pm$ 4.0	144.8 $\pm$ 5.4	143.1 $\pm$ 5.0	152.4 $\pm$ 4.8	149.0 $\pm$ 4.4	119.5 $\pm$ 7.4	115.2 $\pm$ 7.8
Amplitude (deg)	39.1	40.9 $\pm$ 1.2	40.3 $\pm$ 1.2	40.4 $\pm$ 1.2	40.8 $\pm$ 1.3	40.5 $\pm$ 1.2	40.9 $\pm$ 1.2	41.1 $\pm$ 1.3	41.2 $\pm$ 1.3
x-disp (Å)	1.2	0.2 $\pm$ 0.3	0.3 $\pm$ 0.3	0.0 $\pm$ 0.3	-0.3 $\pm$ 0.3	0.3 $\pm$ 0.2	-0.1 $\pm$ 0.3	-2.6 $\pm$ 0.7	-2.93 $\pm$ 0.7
y-disp (Å)	0.0	-0.2 $\pm$ 0.3	-0.2 $\pm$ 0.2	-0.1 $\pm$ 0.3	0.0 $\pm$ 0.3	-0.1 $\pm$ 0.3	0.0 $\pm$ 0.2	0.1 $\pm$ 0.4	0.1 $\pm$ 0.6
Inclination (deg)	-2.9	1.0 $\pm$ 2.4	-0.4 $\pm$ 3.3	3.3 $\pm$ 2.5	0.4 $\pm$ 2.5	-1.5 $\pm$ 2.6	0.7 $\pm$ 2.4	2.1 $\pm$ 5.6	2.6 $\pm$ 6.0
Tip (deg)	0.0	0.8 $\pm$ 2.6	-1.5 $\pm$ 2.2	-0.2 $\pm$ 2.6	0.6 $\pm$ 2.4	-0.5 $\pm$ 2.4	0.2 $\pm$ 2.4	-0.9 $\pm$ 3.1	0.2 $\pm$ 4.2
Shear (Å)	0.0	0.0 $\pm$ 0.1	0.0 $\pm$ 0.1	0.0 $\pm$ 0.1	0.0 $\pm$ 0.1	0.0 $\pm$ 0.1	0.0 $\pm$ 0.0	0.0 $\pm$ 0.0	0.2 $\pm$ 0.3
Stretch (Å)	-0.1	0.1 $\pm$ 0.1	0.1 $\pm$ 0.1	0.1 $\pm$ 0.1	0.1 $\pm$ 0.1	0.1 $\pm$ 0.1	0.1 $\pm$ 0.1	0.2 $\pm$ 0.1	0.2 $\pm$ 0.1
Stagger (Å)	0.0	0.0 $\pm$ 0.1	0.0 $\pm$ 0.1	-0.1 $\pm$ 0.1	-0.2 $\pm$ 0.1	0.1 $\pm$ 0.2	0.0 $\pm$ 0.1	-0.2 $\pm$ 0.1	-0.3 $\pm$ 0.2
Buckle (deg)	0.0	2.6 $\pm$ 4.0	3.7 $\pm$ 4.4	2.1 $\pm$ 3.9	0.2 $\pm$ 3.7	-3.0 $\pm$ 3.9	3.3 $\pm$ 3.8	-0.6 $\pm$ 4.1	-0.1 $\pm$ 4.4
Propeller (deg)	-10.8	-12.6 $\pm$ 2.3	-14.3 $\pm$ 2.3	-13.6 $\pm$ 2.4	-14.2 $\pm$ 2.3	-11.9 $\pm$ 2.4	-13.1 $\pm$ 2.2	-11.3 $\pm$ 3.5	-10.0 $\pm$ 3.6
Opening (deg)	3.0	2.4 $\pm$ 1.4	2.4 $\pm$ 1.4	3.2 $\pm$ 1.5	4.1 $\pm$ 1.5	1.4 $\pm$ 1.5	2.5 $\pm$ 1.4	1.9 $\pm$ 1.5	2.1 $\pm$ 2.0
Shift (Å)	0.0	-0.1 $\pm$ 0.1	-0.1 $\pm$ 0.1	0.0 $\pm$ 0.1	0.1 $\pm$ 0.1	0.0 $\pm$ 0.1	-0.1 $\pm$ 0.1	0.0 $\pm$ 0.1	0.0 $\pm$ 0.1
Slide (Å)	0.4	0.0 $\pm$ 0.1	-0.1 $\pm$ 0.1	0.0 $\pm$ 0.1	-0.1 $\pm$ 0.1	0.0 $\pm$ 0.1	0.0 $\pm$ 0.1	-0.2 $\pm$ 0.1	-0.2 $\pm$ 0.1
Rise (Å)	3.4	3.5 $\pm$ 0.1	3.5 $\pm$ 0.1	3.5 $\pm$ 0.1	3.5 $\pm$ 0.1	3.4 $\pm$ 0.1	3.5 $\pm$ 0.1	3.3 $\pm$ 0.2	3.3 $\pm$ 0.2
Tilt (deg)	0.0	0.9 $\pm$ 1.3	-0.2 $\pm$ 1.1	0.2 $\pm$ 1.3	0.1 $\pm$ 1.1	-0.1 $\pm$ 1.2	0.7 $\pm$ 1.2	-0.3 $\pm$ 1.3	0.3 $\pm$ 2.0
Roll (deg)	2.1	2.8 $\pm$ 1.2	3.0 $\pm$ 1.5	2.3 $\pm$ 1.2	3.3 $\pm$ 1.3	4.2 $\pm$ 1.1	3.6 $\pm$ 1.1	3.9 $\pm$ 1.7	4.7 $\pm$ 2.1
Twist (deg)	35.5	34.1 $\pm$ 0.5	35.3 $\pm$ 0.6	34.8 $\pm$ 0.5	34.7 $\pm$ 0.5	33.2 $\pm$ 0.5	33.3 $\pm$ 0.5	30.5 $\pm$ 1.2	30.4 $\pm$ 1.5

Data derived from the crystal structure are under the column heading 5 dnB. The two duplexes in the one unit cell crystal simulation are denoted One-1 and One-2. The four duplexes from the two unit cell crystal simulation are denoted Two-1 through Two-4. The solution simulation starting from canonical B-DNA is denoted Solution (Canonical), and that starting from the crystal structure, Solution (Crystal). Data from the MD simulations were obtained by averaging over the following time periods: one unit cell crystal simulation, 20–25 ns; two unit cell crystal simulation, 10–15 ns; solution simulation starting from canonical B-DNA, 10–12 ns; solution simulation starting from the crystal structure, 4–5 ns.

simulation. This long simulation allows for a careful analysis of the stability of the trajectory. Notably, the RMS deviation of Duplex 1 was relatively stable during the last 7

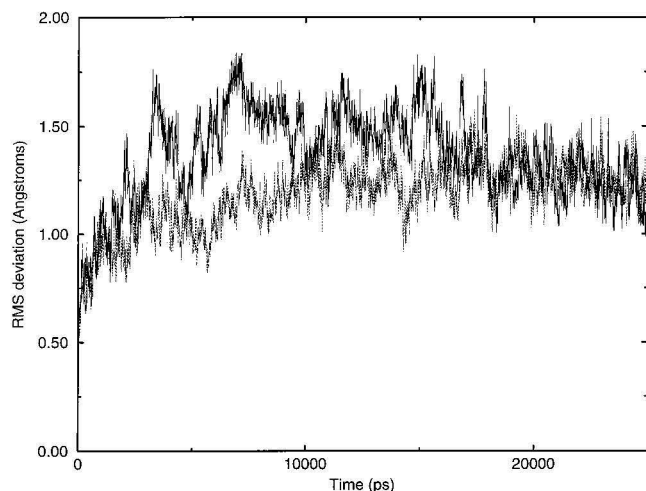


**FIGURE 2** RMS deviations of the duplexes in the one unit cell simulation. The solid line represents the data for the duplex denoted One-1, and the dashed line, One-2. Data points were collected at 1-ps intervals during the trajectory, and data have been smoothed by performing a 50-point running average in time before plotting.

ns of the simulation, although considerable fluctuation in RMS deviation was noted earlier in the trajectory. Duplex 2 was relatively stable for the last 15 ns of the simulation. The RMS deviations of the duplexes were very similar to one another by the end of the trajectory.

Analysis of the helicoidal parameters of each duplex in the one unit cell simulation, calculated over the last 5 ns of the simulation, shows only small differences between the duplexes (Table 1), as might be expected based on their similar RMS deviations. These differences are most apparent in the backbone torsional parameters, with small differences in one torsional parameter being compensated for by small differences in other torsional parameters, such that the overall RMS deviations for the two duplexes in the one unit cell crystal simulation are nearly identical (Table 2).

It also was of interest to determine if obvious structural differences were apparent when the RMS deviations of the duplexes were not similar. Helicoidal parameters of duplexes 1 and 2, calculated over the 5–10-ns time interval, did not differ substantially from one another or from the parameters calculated during the 20–25-ns time interval (data not shown). These results indicate that RMS deviations may be a relatively insensitive indicator of differences among these structures.



**TABLE 2** RMS deviations of the structures from the molecular dynamics simulations relative to the crystal structure

Structure	RMS deviation (Å)
One-1	1.18
One-2	1.15
Two-1	1.00
Two-2	1.48
Two-3	1.25
Two-4	1.48
Solution (canonical)	3.65
Solution (crystal)	4.22

Definitions of the row labels are given in Table 1. Structures from the MD simulations were obtained by averaging over the following time periods: one unit cell crystal simulation, 20–25 ns; two unit cell crystal simulation, 10–15 ns; solution simulation starting from canonical B-DNA, 10–12 ns; solution simulation starting from the crystal structure, 4–5 ns. Solvated structures were minimized, first by minimizing Na<sup>+</sup> and water molecules only (300 steps steepest descents) and then the entire system (600 steps steepest descents). RMS deviations of the duplexes (heavy atom positions) were calculated relative to the crystal structure (5dnb).

#### Two unit cell simulation

In Fig. 3 are the RMS deviations for the simulation involving four duplexes in two unit cells. During the first 2.5 ns, the RMS deviations were similar for all of the duplexes, and the system appeared to be relatively stable. Shortly thereafter, larger differences in RMS deviation were noted among the duplexes, and these differences persisted, even out to 15 ns. Examination of the helicoidal parameters for these duplexes (Table 1) reveals some differences, especially in the backbone torsion angles.

#### Comparison of crystal and solution simulations

The RMS deviations of the solution simulations suggested that a stable trajectory was attained within 4 ns, which is faster than in the crystal simulations (data not shown). It is possible that the crystal environment imposes constraints that increase the time required to achieve stability. The RMS deviations of the DNA duplexes in the crystal and solution simulations relative to the crystal structure are given in Table 2. It is seen that the structures from the solution simulations deviated considerably more from the crystal structure than did those from the crystal simulations. Notably, the values of RMS deviation in the solution simulations are in the range of the RMS deviations reported by Cheatham and Kollman (1996).

A more critical comparison of the structures can be made by considering the helicoidal parameters listed in Table 1. The results for several of the helicoidal parameters are particularly notable when the parameters from the crystal and solution simulations are compared with one another and with parameters for the crystal structure. These parameters include  $\alpha$ ,  $\gamma$ ,  $\delta$ ,  $\epsilon$ ,  $\zeta$ , phase, and twist. Each of these parameters will be examined in more detail.

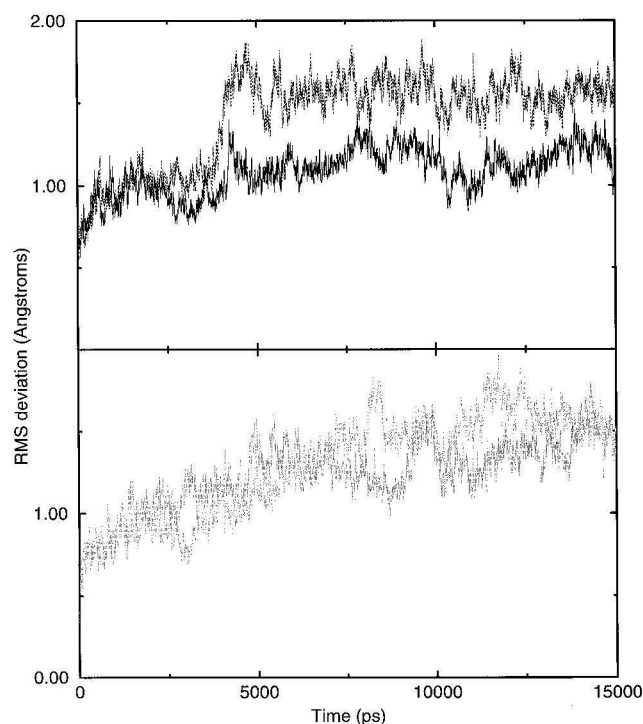


**FIGURE 3** RMS deviations of the duplexes in the two unit cell simulation. Duplexes Two-1 (black solid line) and Two-2 (black dashed line) are in the upper half of the figure, and duplexes Two-3 (gray solid line) and Two-4 (gray dashed line) are in the lower half. Data points were collected at 1-ps intervals during the trajectory, and data have been smoothed by performing a 50-point running average in time before plotting.

#### $\alpha$ and $\gamma$

In Table 1 it is seen that values for the torsional angle  $\alpha$  from the crystal simulations are consistently much lower than the value of  $\alpha$  from the solution simulations or the crystal structure. These low values of  $\alpha$  appear to be compensated for by the consistently higher values of the  $\gamma$  torsion angle. The correlation between  $\alpha$  and  $\gamma$  is more apparent from Fig. 4, in which values of  $\alpha$  and  $\gamma$  from the solution simulation starting from the canonical structure and the one unit cell crystal simulation are shown. A number of points can be made regarding the data in Fig. 4. First, changes in  $\alpha$  and  $\gamma$  appear to correlate well—as  $\alpha$  decreases,  $\gamma$  increases. Second, discrete changes in values of  $\alpha$  and  $\gamma$  are observed during the simulations, suggesting that changes among distinct structural forms are occurring. If a steady decline in  $\alpha$  and a steady increase in  $\gamma$  had been observed over the course of the simulations, we would have attributed the change to a force-field-related problem. Third, the differences in values reported in Table 1 are dependent on the time frame used to calculate the average structural properties. For the solution simulation starting from the canonical structure, we used 10–12 ns; for the one unit cell crystal simulation, we used 20–25 ns. Values of  $\alpha$  during the crystal simulation were lowest during that time period.



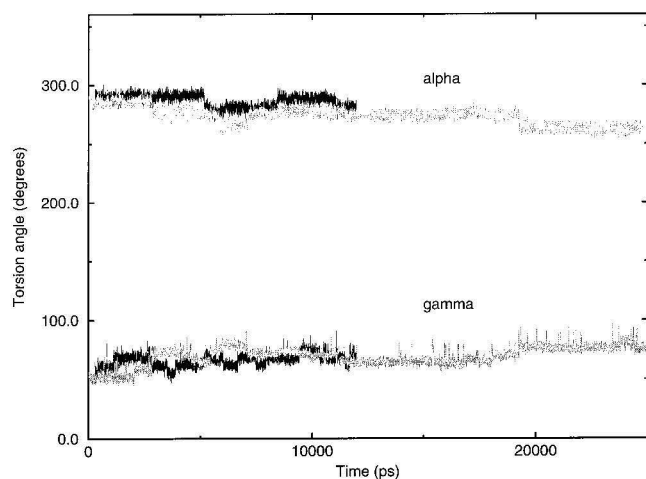


FIGURE 4 Changes in torsion angles  $\alpha$  and  $\gamma$  during the trajectories. Black lines correspond to results from the solution simulation starting from canonical B-DNA, and gray lines to results from the one unit cell crystal simulation.

During the 10–12-ns time period in the solution simulation, values of  $\alpha$  were relatively high, and lower values were observed during the 5–8-ns time period.

#### $\delta$ and phase angle

For  $\delta$  and the pseudorotation phase angle, the crystal simulations gave much better agreement with the crystal structure than did the solution simulations. It is generally accepted that the  $\delta$  torsion, being part of the deoxyribose ring, correlates with the pseudorotation phase angle (Dickerson, 1992). Thus we will not discuss  $\delta$  in our more detailed analysis but rather consider the pseudorotation phase angle, which includes  $\delta$  as one of its components. We analyzed changes in the pseudorotation phase angle, which provides an analysis of the sugar repuckering, over the course of the trajectories. From Fig. 5 it is seen that during the simulations, the sugar conformation is most frequently C2'-endo (phase angle = 137°–194°), although transitions to C3'-endo (phase angle = -1°–34°) are observed. Repuckering tends to occur more often during the solution simulation than in the crystal simulation. In fact, the example chosen for illustration of the crystal simulations showed the greatest frequency of transition among the duplexes in either of the crystal simulations, although some repuckering was observed in all of the duplexes. As is apparent from Fig. 5, when transitions occurred during the crystal simulations, the sugar rings tended to stay in the newly adopted conformation for an extended period, unlike transitions in the solution simulations. This observation of less frequent repuckering during the crystal simulation would explain the close agreement between the value of the phase angle in the crystal simulations and the crystal structure. That is, if frequent repuckering to C3'-endo were to occur, as in the solution

simulation, then the average value of the phase angle would be correspondingly lower. Moreover, the value of the phase angle reported in Table 1 is an average over all residues. In the crystal simulation, the repuckering occurred principally in one residue, T-8, and the phase for other residues in the crystal simulations tended to be higher than that for the corresponding residues in the solution simulation. These differences in repuckering between the solution and crystal simulations may reflect constraints imposed by crystal packing, although it is clear that repuckering can still occur during the crystal simulations. These crystal packing constraints may overcome force-field deficiencies such that better agreement with the crystal structure is obtained.

#### $(\epsilon - \zeta)$

From Table 1 it is seen that values of  $\epsilon$  for the structures in the crystal simulations are generally somewhat higher than that for the crystal structure, and the values in the solution simulations are comparably lower. Values of  $\zeta$  in the crystal simulation are similar to that in the crystal structure, but those in the solution simulations are considerably higher. The difference  $(\epsilon - \zeta)$  is often used when these values are analyzed, because it assumes values that are characteristic of the BI backbone conformation (-90°) and the BII backbone conformation (+90°) (Lavery, 1994). In the crystal structure, the values of  $(\epsilon - \zeta)$  for C-2 and T-8 are indicative of the BII conformation, while the others are characteristic of the more common BI conformation. Notably, in the solution simulations, all values are indicative of the BI conformation. In the crystal simulations, some of the duplexes retain values of  $(\epsilon - \zeta)$  at positions C-2 and T-8 that are characteristic of the BII conformation (data not shown).

We have examined values of  $(\epsilon - \zeta)$  as a function of time. Shown in Fig. 6 are results from the solution simulation starting from the canonical B-DNA structure, and in Fig. 7 are results from one of the crystal simulations. The results from the solution simulation illustrate that transitions between BI and BII occur, albeit relatively infrequently. This is most apparent at residue A-4. In the crystal simulation, frequent transitions are observed at several bases, including C-2 and T-8. Note that the example in Fig. 7 was chosen because it illustrates frequent transitions. For other DNA strands in the crystal simulations, the transitions were not as frequent. However, it is important to recognize that the crystal environment does not overly constrain the DNA duplexes such that they remain rigid in the crystal lattice during the simulation. Rather, flexibility is apparent, based on the transitions illustrated here.

#### Helical twist

Perhaps most interesting among the helicoidal parameters are the values for helical twist. Solution simulations of DNA



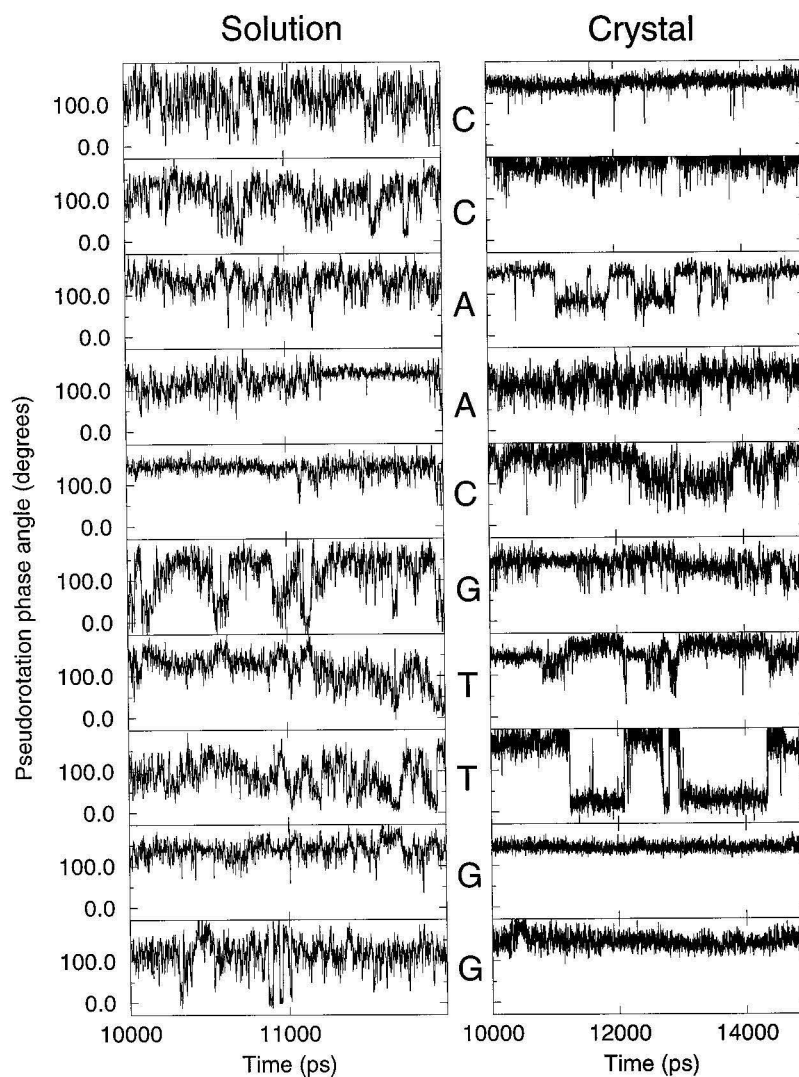


FIGURE 5 Changes in pseudorotation phase angle for the deoxyribose sugars in each nucleotide during the trajectories. The solution results are from the simulation beginning from canonical B-DNA, and the results are for strand 1 of the duplex. The crystal results are from the two unit cell simulation and are for strand 2 of duplex Two-1.

with the Cornell et al. (1995) force field typically result in an undertwisting of the duplex, such that values for twist are lower than those observed in crystal structures (Cheatham and Kollman, 1996, 1997; Cieplak et al., 1997; Young et al., 1997b). This phenomenon also is apparent in our results (Table 1). In contrast, the twist parameter values for the crystal simulations are higher than for the solution simulation and are very close to that in the crystal structure. This result may derive from the constraints placed upon the DNA duplexes within the unit cell.

Helical twist is also of interest because it appears to be sequence dependent (El Hassan and Calladine, 1997; Gorin et al., 1995). For some of the other parameters that are reported to show some sequence dependence (e.g., roll, slide, propeller), the standard deviation (fluctuation) over the course of the simulations was sufficiently large that we could not discern a sequence dependence. Moreover, some of the sequence dependence of DNA structural features deduced from crystal structures has recently been attributed

to experimental error in the crystal structure determinations (Shui et al., 1998a). In our simulations, the values of helical twist are sufficiently large and the fluctuations sufficiently small that some sequence dependence may be apparent. To examine the sequence dependence of helical twist in the simulations, values were determined for each base step (Table 3). Notably, the values of twist at each base step in the crystal simulations correspond well to the values in the crystal structure. That is, the sequence dependence of helical twist was maintained in the crystal simulations. However, values of helical twist in the solution simulations were uniformly close to  $30^\circ$ . Because the sequence dependence of helical twist was not preserved in the solution simulations, we examined the time course over which the helical twist changed in the solution simulation starting from the crystal structure. In Fig. 8 is shown the decrease in helical twist for the three base steps that have the highest values in the crystal structure. The helical twist for two of the base steps decreased to around  $30^\circ$  within the first 250 ps of the



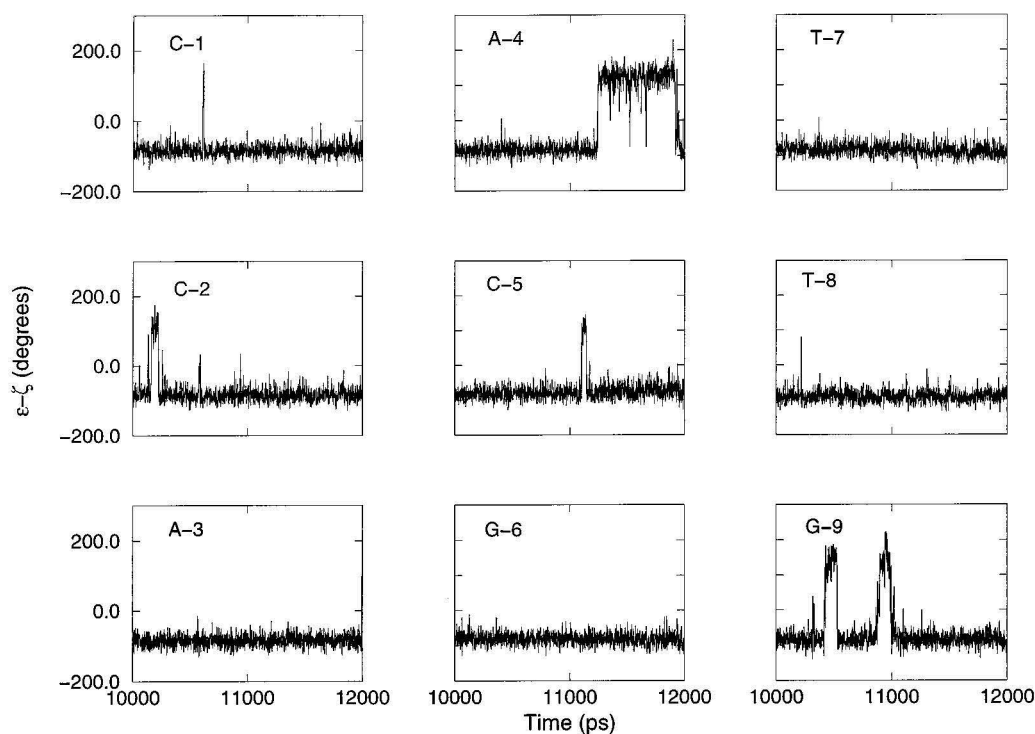


FIGURE 6 Changes in  $(\epsilon-\zeta)$  at each nucleotide during the solution simulation starting from canonical B-DNA. Results are illustrated for strand 1 of the duplex.

trajectory, and the helical twist for the third base step decreased within 1 ns.

#### Minor groove width

Another parameter that is reported to exhibit some sequence dependence is minor groove width (Boutonnet et al., 1993; Nelson et al., 1987; Sarma et al., 1997). A comparison of minor groove widths from the simulations with that of the crystal structure is given in Fig. 9. The minor groove width is not precisely preserved in any of the simulations. However, it is apparent that a narrowing of the minor groove as observed in the crystal structure is seen in the crystal simulations but not the solution simulations. The time dependence over which the minor groove width increased in the solution simulation starting from the crystal structure was determined (Fig. 10). Considerable fluctuation in minor groove width was observed during the trajectory, but it appears to be stabilizing in its wider state by  $\sim 4$  ns into the simulation.

#### Analysis of B-factors

Another means of comparing the results of MD simulation with the crystal structure is to calculate B-factors and compare them to the crystallographic B-factors. The B-factors provide a measure of the fluctuation at atomic positions

within the DNA molecules. In Fig. 11, calculated B-factors from the one unit cell simulation and the solution simulation starting from the canonical structure are compared to the B-factors from crystallography. For clarity, each strand of DNA from the one unit cell simulation is depicted in a separate panel (Fig. 11, *A–D*). As expected, the regions of highest atomic fluctuation are in the backbone atoms. Agreement between calculated and experimental B-factors varies among the four strands in the one unit cell simulation. The closest agreement is observed in Fig. 11, *B* and *D*. In Fig. 11, *A* and *C*, the calculated results suggest regions of less atomic fluctuation than in the experiment. We also calculated B-factors from a solution simulation (Fig. 11 *E*). Clearly, the magnitude of the fluctuations is greater in the solution simulation than in the crystal simulation or in the experiment. However, the agreement between regions undergoing greater and lesser atomic fluctuation is good when calculated and experimental values are compared.

#### Mg<sup>2+</sup>, water structure, and dynamics

It also was of interest to consider the structural relationships among the Mg<sup>2+</sup> ions, water molecules, and DNA during the crystal simulations to determine if these components behaved as expected. The water molecules that constituted the hydration sphere around each Mg<sup>2+</sup> ion were examined for the crystal structure and for structures at various times

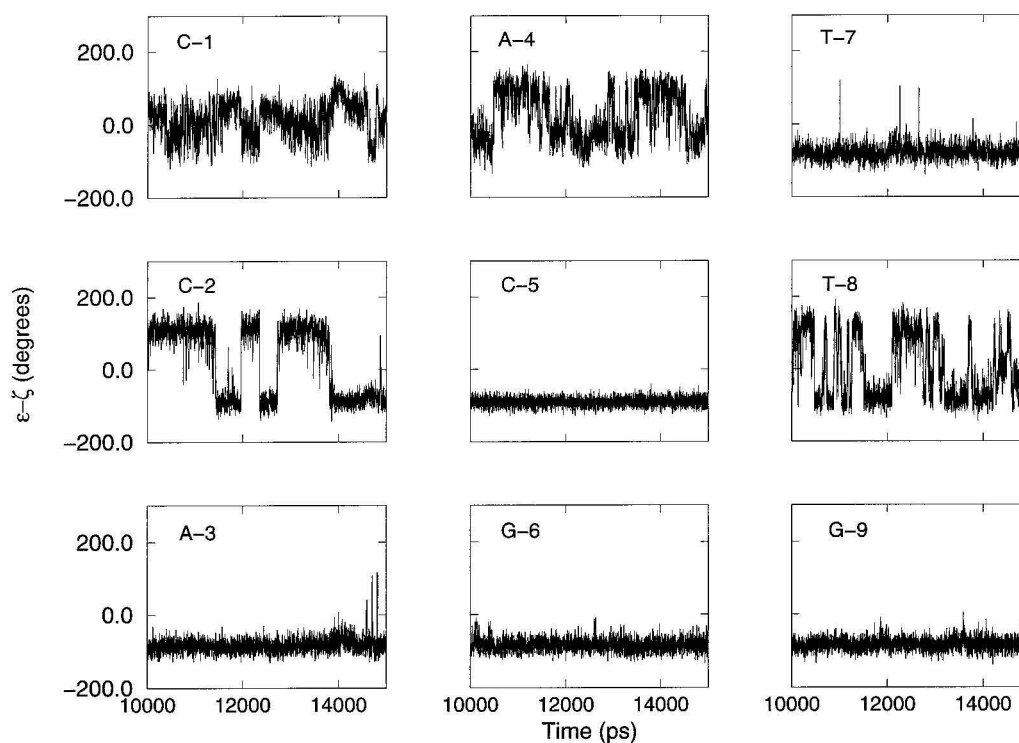


FIGURE 7 Changes in  $(\epsilon - \zeta)$  at each nucleotide during a crystal simulation. Results are from strand 2 of duplex Two-2 in the two unit cell simulation.

during the one unit cell crystal simulation. In only two cases was an exchange of water molecules observed within the primary coordination sphere. That is, the water molecules constituting the primary sphere of hydration tended not to exchange with the bulk solvent. The radial distance distribution of water molecules relative to  $\text{Mg}^{2+}$  ions was determined for the last 5 ns of the one unit cell trajectory (Fig. 12). It is clear that the  $\text{Mg}^{2+}$  ions maintain the hydration shell, with the molecules in the inner sphere 2.0–2.1 Å from the  $\text{Mg}^{2+}$  and those in the outer sphere 4.1–4.3 Å from the  $\text{Mg}^{2+}$  (Bock et al., 1994).

Analysis of the trajectories revealed that some of the  $\text{Mg}^{2+}$  ions (with their associated sphere of hydration) moved relative to the DNA molecules. An example of the

extent of this movement is given in Fig. 13, in which the position of a  $\text{Mg}^{2+}$  ion relative to nearby DNA phosphorus atoms is illustrated. The motion is characterized by small fluctuations around equilibrium positions with a few larger abrupt changes in position. When viewed as a radial distribution function, the  $\text{Mg}^{2+}$ -P distances show a primary distance of  $\sim 4.9$  Å, which is characteristic of a system in which the  $\text{Mg}^{2+}$  hydration sphere is maintained and no direct  $\text{Mg}^{2+}$ -P bonding occurs (data not shown).

## DISCUSSION

Our crystal simulations appear to provide a reasonable representation of the crystal environment in the unit cell.

TABLE 3 Helical twist as a function of base step

Base step	5dnb	One-1	One-2	Two-1	Two-2	Two-3	Two-4	Solution (canonical)	Solution (crystal)
CC	29.1	28.0 ± 3.4	27.2 ± 3.6	20.7 ± 3.9	36.6 ± 3.2	19.9 ± 3.1	29.0 ± 3.8	30.2 ± 4.6	29.9 ± 4.3
CA	48.9	49.6 ± 2.8	44.1 ± 3.0	46.7 ± 3.5	43.8 ± 3.3	47.9 ± 2.4	48.0 ± 2.6	30.8 ± 4.1	29.3 ± 4.8
AA	29.8	27.9 ± 3.1	37.5 ± 2.6	31.8 ± 3.2	25.6 ± 3.7	26.9 ± 3.8	29.5 ± 2.9	28.3 ± 4.8	29.1 ± 5.8
AC	31.5	23.8 ± 3.1	30.6 ± 3.0	27.0 ± 3.5	35.8 ± 4.9	27.1 ± 3.1	27.2 ± 3.1	30.7 ± 4.5	29.3 ± 4.1
CG	39.2	41.8 ± 3.4	43.4 ± 3.4	42.8 ± 3.9	29.0 ± 4.4	44.1 ± 3.6	41.1 ± 4.1	29.7 ± 5.8	30.2 ± 4.2
GT	31.5	36.1 ± 4.6	34.3 ± 3.5	33.0 ± 4.0	38.3 ± 3.2	31.4 ± 4.7	28.1 ± 3.5	32.9 ± 4.6	28.4 ± 3.6
TT	29.8	21.6 ± 5.0	32.0 ± 3.4	29.2 ± 4.0	29.8 ± 3.4	29.1 ± 4.8	30.8 ± 3.2	32.8 ± 5.7	28.9 ± 4.0
TG	48.9	47.5 ± 2.8	41.9 ± 2.8	46.9 ± 2.7	44.8 ± 4.9	48.8 ± 3.0	46.0 ± 2.7	27.8 ± 6.2	31.2 ± 4.4
GG	29.1	30.7 ± 3.6	26.5 ± 5.2	34.9 ± 2.8	28.8 ± 5.0	23.8 ± 4.3	20.0 ± 2.8	31.4 ± 5.2	37.1 ± 10.7

Definitions of the column headings are given in Table 1. Values for helical twist are in degrees. Values for the helical twist from the simulations were obtained by averaging over the following time periods: one unit cell crystal simulation, 20–25 ns; two unit cell crystal simulation, 10–15 ns; solution (canonical), 10–12 ns; solution (crystal), 4–5 ns.



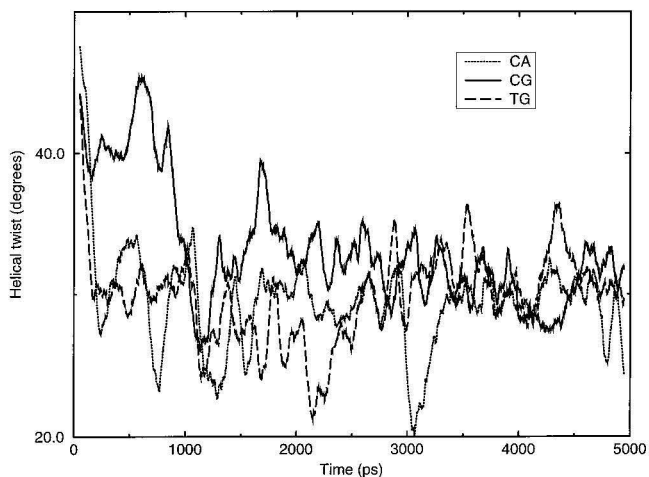


FIGURE 8 Changes in helical twist during the solution simulation starting from the crystal structure. Results are illustrated for the three base steps that have the highest values of helical twist in the crystal structure. Data were smoothed by performing a 100-point running average in time.

Under constant-pressure MD conditions, the volume of the unit cell during the last 5 ns of the one unit cell simulation was  $26,286 \pm 140 \text{ \AA}^3$ , which agrees reasonably well with the published value of  $25,980 \text{ \AA}^3$  (Prive et al., 1991). That the box size stayed essentially constant during MD indicates that we had included the appropriate number of bulk water molecules, in addition to the DNA,  $\text{Mg}^{2+}$  ions, and crystallographic water molecules, to simulate the crystal environment.

One of our simulations, the solution simulation starting from the canonical B-DNA structure, replicates the work of Cheatham and Kollman (1996), though our simulation was carried out for a considerably longer period of time (12,000 ps versus 1456 ps). Our results for mean values of helicoidal parameters are in excellent agreement with those of Cheatham and Kollman (1996), although our standard deviations typically were considerably lower. Although we averaged over a longer time period (2000 ps versus 856 ps), it is unlikely that the magnitude of this difference is large enough to explain the different values for standard deviations. The difference in standard deviations most likely results from different methods of data analysis. For example, in our calculations reported in Table 1, we calculated an average value for each parameter in each structure of the trajectory and then calculated a mean and standard deviation based on these average values from all of the structures. An alternative is to calculate averages of individual residues, base pairs, or base-pair steps (Cheatham and Kollman, 1996). Nevertheless, a careful comparison of our data with those of other investigators indicates that the range of values observed over the course of a trajectory is similar. Thus, we conclude that our solution simulation conditions and results are comparable to those reported previously.

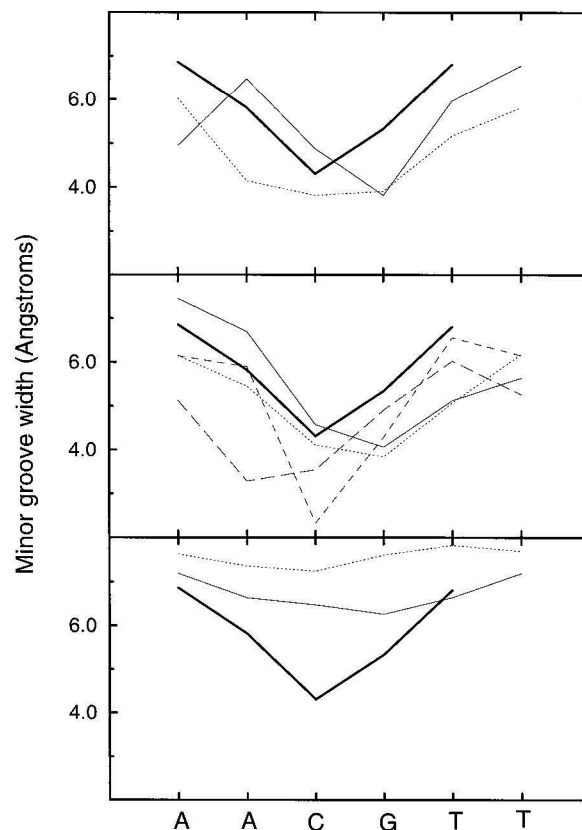


FIGURE 9 Minor groove widths in the central part of the duplexes from the crystal and solution simulations. In all graphs, the heavy black line illustrates the minor groove width for the crystal structure (5dnb). (Top) One unit cell crystal simulation. (Middle) Two unit cell crystal simulation. (Bottom) Solution simulations. Results shown were obtained by averaging over the following time periods: one unit cell crystal simulation, 20–25 ns; two unit cell crystal simulation, 10–15 ns; solution simulation starting from canonical B-DNA, 10–12 ns; solution simulation starting from the crystal structure, 4–5 ns.

When comparing the helicoidal parameters from our crystal and solution simulations with one another and with the crystal structure, we see that differences are most apparent in the parameters  $\alpha$ ,  $\gamma$ ,  $\epsilon$ ,  $\zeta$ , phase, and helical twist. For many of the other parameters, the absolute values are close to zero and the standard deviations are sufficiently high that differences cannot be discerned. The correlated crankshaft motion involving  $\alpha$  and  $\gamma$  is expected in that it has been observed in other MD simulations (Swaminathan et al., 1991; Cheatham and Kollman, 1997) and in NMR studies (Xu et al., 1998). As noted above, the abrupt changes in  $\alpha$  and  $\gamma$  suggest that rapid transitions among similar structures are occurring and that all structures are energetically favorable. Notably, significant changes in RMS deviation were not observed when  $\alpha$  and  $\gamma$  changed abruptly, suggesting that in terms of the overall structure, the small changes in  $\alpha$  were balanced by small changes in  $\gamma$ . Differences between values of  $\alpha$  and  $\gamma$  in the crystal simulations and those in the solution simulations would suggest

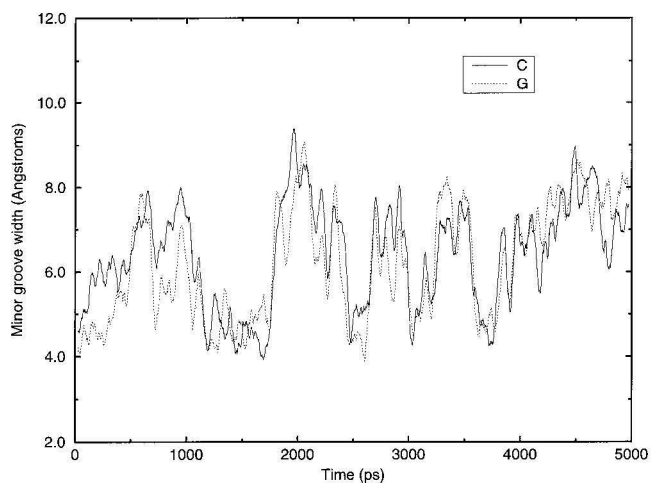


FIGURE 10 Change in minor groove width during the solution simulation starting from the crystal structure. Results are shown for the minor groove width at the bases in the middle of the decamer (C and G).

some constraint due to crystal packing forces, while differences in these values relative to the crystal structure would suggest some deficiency in the force field. This problem with the force field is also apparent from the observation that the lower average values of  $\alpha$  and higher values of  $\gamma$  relative to the crystal structure reflect to some extent the time period over which structures were averaged. From Fig. 4 we can see that if averaging in the one unit cell crystal simulation were to be carried out over the 10–12-ns time period, as was done for the solution simulation, values of  $\alpha$  and  $\gamma$  would be much closer to those from the solution simulation and the crystal structure.

From analysis of the time dependence of  $\alpha$  and  $\gamma$ , as well as other parameters, we do not think that the DNA was overly constrained during the crystal simulations. For example, BI to BII backbone transitions were apparent in the crystal simulations, just as in solution simulations. Sugar repuckering also occurs in the crystal simulation, although the rings near the ends of the duplex appear to be more tightly constrained than those toward the middle of the duplex, a finding that is not observed in the solution simulations. From the B-factors, it also appears that DNA in the crystal simulation is somewhat less flexible than that in the solution simulations, suggesting that the tighter packing within the simulated crystal is constraining movement to some extent. However, the close agreement between B-factors from the crystal simulations and those from the crystal structure suggests that the conditions for our crystal simulations, along with the force field of Cornell et al. (1995), accurately represent the dynamics of the duplex in the crystal environment.

Our analysis of helical twist and minor groove width make apparent some problems associated with solution simulations of DNA. Other investigators also have noted that the average value for overall helical twist decreases to  $\sim 30^\circ$

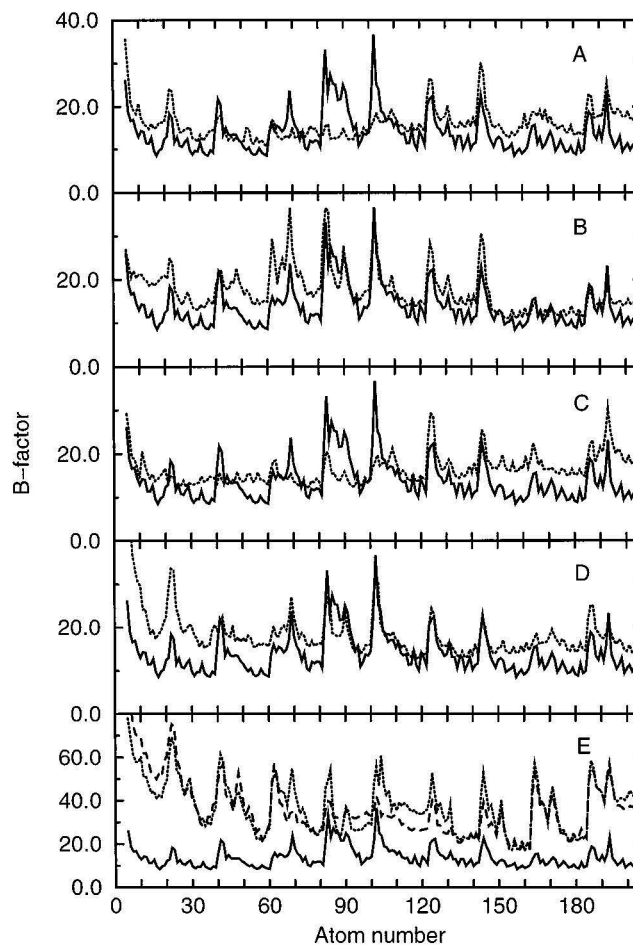


FIGURE 11 B factors calculated from the simulations compared with B factors from the crystal structure. In each panel, the dark solid line illustrates the B factors from the crystal structure. Results from the one unit cell simulation are shown for strand 1 of duplex 1 (A), strand 2 of duplex 1 (B), strand 1 of duplex 2 (C), and strand 2 of duplex 2 (D). Results for the solution simulations are given in E for the simulations starting from canonical B-DNA (dotted line) and from the crystal structure (dashed line).

during solution simulations (Cheatham and Kollman, 1996, 1997; Cieplak et al., 1997; Young et al., 1997b). The dependence of helical twist on base step in MD simulations has been less thoroughly analyzed. Duan et al. (1997), in a 1-ns simulation of the dodecamer duplex  $d(\text{CGCGAAT-TCGCG})_2$ , reported an unwinding of the duplex and a convergence of twist angles to  $\sim 33^\circ$  within the first 500 ps of their 1-ns simulation. The average value of helical twist may decrease even further in a longer simulation. In any case, our result is consistent with theirs in that differences in helical twist as a function of base step are not apparent in solution simulations. The loss of this sequence-dependent information is a problem that must be resolved if solution MD simulations are to be used in a predictive way to understand the relationship between DNA sequence and structure. That we were able to preserve this sequence-dependent information, even in extremely long crystal MD



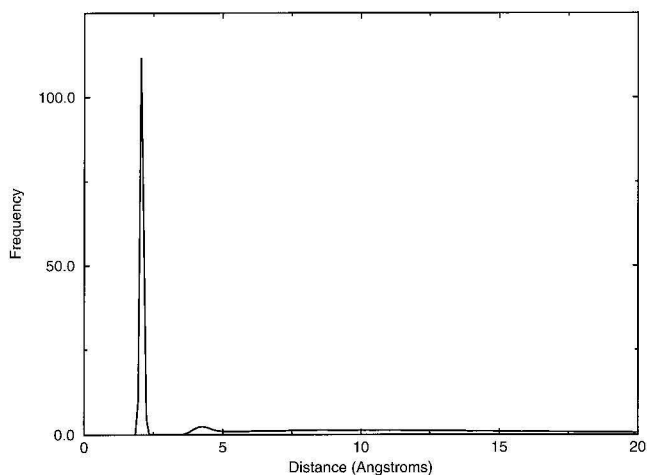


FIGURE 12  $Mg^{2+}$ -water oxygen radial distribution function (normalized) calculated from the one unit cell simulation. Data from the time period 20–25 ns were used in the calculation.

simulations, suggests that these crystal simulations may provide a tool for analyzing the variables within the solution simulations that account for the decrease in helical twist. Moreover, Cheatham et al. (1999) have recently released a modified version of the force field of Cornell et al. in which improved values for pseudorotation phase angle and helical twist are observed in solution simulations. We intend to apply this modified force field to our simulations in the future.

The minor groove width also shows sequence dependence (Boutonnet et al., 1993; Nelson et al., 1987; Sarma et al., 1997) and thus merits careful scrutiny in MD simulations. We noted that some narrowing of the minor groove is apparent in all of the duplexes in our crystal simulations,

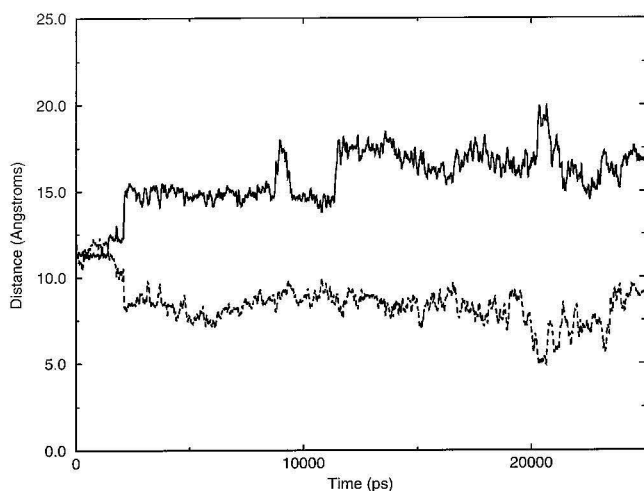


FIGURE 13 Distance between  $Mg^{2+}$ -45 and phosphorus DNA atoms during the one unit cell trajectory. Distances are between  $Mg^{2+}$ -45 and T7P (—) and A14P (---). Data were smoothed by performing a 50-point running average in time.

although we clearly have not maintained the minor groove width of the crystal structure precisely. In our solution simulations, little narrowing of the minor groove is observed. In the simulations of Cheatham and Kollman (1996, 1997) of the d(CCAACGTTGG)<sub>2</sub> decamer, the minor groove width was narrowed, but not to the same extent as in the crystal structure. In the study by Duan et al. (1997) of the Dickerson dodecamer starting from the “bent” crystal structure, the duplex appeared to retain some narrowing within the minor groove, although the simulation was performed for only 1 ns. In a 5-ns simulation of the Dickerson dodecamer starting from canonical B-DNA, Young et al. (1997a) noted a slight narrowing of the minor groove, though not to the same extent as seen in the crystal structure. The differences observed among these studies probably result from the different sequences under investigation and from different simulation conditions. In particular, as we have illustrated in Fig. 10, the minor groove width changes with time, with a narrow minor groove more likely to be observed on shorter time scales (e.g., <1.5 ns) when we start from a crystal structure with a narrow minor groove.

The behavior of the  $Mg^{2+}$  ions during the crystal simulations also needs to be considered because it is recognized that metal ions may have a significant influence on DNA structure (Saenger, 1984). In our crystal simulations, the  $Mg^{2+}$  ions from the crystal structure were included, with eight  $Na^+$  ions needed to achieve electroneutrality. We were most interested in the behavior of the  $Mg^{2+}$  ions during the simulations and analyzed their positions relative to the DNA as a function of time. In addition,  $Na^+$  ions generally are considered to be very diffusible, although they are reported to form inner sphere complexes with DNA (Westhof et al., 1995). Recent studies support this observation. For example, Young et al. (1997a) observed that  $Na^+$  ions are incorporated within the primary hydration sphere of the minor groove of d(CGCGAATTCGCG)<sub>2</sub>, from which they suggest that  $Na^+$  ions may function as an extrinsic source of sequence-dependent effects on DNA structure. This observation was reinforced by studies of Shui et al. (1998a,b). In a high-resolution crystal structure of d(CGCGAATTCGCG)<sub>2</sub>, they noted that  $Na^+$  ions penetrated the spine of hydration in the minor groove (Shui et al., 1998a). They subsequently confirmed this observation in a structure of the dodecamer in the presence of  $K^+$  ions, which are easier to distinguish from water molecules than are  $Na^+$  ions (Shui et al., 1998b).

The coordination of divalent cations is hypothesized to occur in two ways. First, an outer sphere complex can form; then, with the loss of one or more water molecules, an inner sphere complex can form (Westhof et al., 1995). However,  $Mg^{2+}$  ions are reported to form inner sphere complexes at a relatively low rate ( $\sim 10^5 s^{-1}$ ) and primarily with short polyadenylate chains (Porschke, 1978). Cowan et al. (1993), using <sup>25</sup>Mg NMR spectroscopy, determined that binding of  $Mg^{2+}$  ions to DNA involves outer sphere complexes with



$\text{Mg}(\text{H}_2\text{O})_6^{2+}$  and that binding to G/C-rich sequences occurs with 40- to 100-fold higher affinity than binding to A/T-rich sequences. Similarly, Shui et al. (1998b) made a survey of complexes between  $\text{Mg}^{2+}$  ions and B-DNA in the Nucleic Acid Data Bank (Berman et al., 1992) and noted that when  $\text{Mg}^{2+}$  ions are bound to DNA, they remain fully hydrated and interact with DNA through water molecules in the first hydration shell. However, in a recent high-resolution (1.1 Å) crystal structure of  $(\text{CGCGAATTCGCG})_2$  most of the contacts between  $\text{Mg}^{2+}$  ions and DNA were mediated by water molecules, but two direct contacts between the ions and DNA were observed (Tereshko et al., 1999). Moreover, when Buckin et al. (1994) applied ultrasonic titration experiments in the analysis of  $\text{Mg}^{2+}$ -DNA binding, they concluded that  $\text{Mg}^{2+}$  ions form outer sphere complexes with oligomers containing dA-dT base pairs and inner sphere complexes with dG-dC base pairs.

In MD simulations in which  $\text{Mg}^{2+}$  ions are present, the ions exist primarily as hexahydrates (Lee et al., 1995b; MacKerrell, 1997). Considering the length of the simulations and the relatively slow exchange rate for  $\text{H}_2\text{O}$  bound to  $\text{Mg}^{2+}$  ions noted above, it is likely that inner sphere coordination would not be observed. However, in the simulations of Lee et al. (1995b), two of the  $\text{Mg}^{2+}$  ions were hypothesized to exist in a complex in which the ions were bridged by hydroxide ions. Clearly, additional studies are required to understand binding of  $\text{Mg}^{2+}$  ions to DNA and the effect on DNA structure, which is a research problem that we continue to pursue.

DRB thanks the National Institute of Environmental Health Science (NIEHS) for partial support of a sabbatical year. LGP thanks the North Carolina Supercomputing Center for a grant of computer time and the National Institutes of Health for grant HL-06350. This research was performed while DRB was on study-research leave at the NIEHS.

## REFERENCES

- Berman, H. M., W. K. Olson, D. L. Beveridge, J. Westbrook, A. Gelbin, T. Demeny, S.-H. Hsieh, A. R. Srinivasan, and B. Schneider. 1992. The nucleic acid database. A comprehensive relational database of three-dimensional structures of nucleic acids. *Biophys. J.* 63:751-759.
- Bock, C. W., A. Kaufman, and J. P. Glusker. 1994. Coordination of water to magnesium ions. *Inorg. Chem.* 33:419-427.
- Boutonnet, N., X. Hui, and K. Zakrzewska. 1993. Looking into the grooves of DNA. *Biopolymers.* 33:479-490.
- Buckin, V. A., B. I. Kankiya, D. Rentzperis, and L. A. Marky. 1994.  $\text{Mg}^{2+}$  recognizes the sequence of DNA through its hydration shell. *J. Am. Chem. Soc.* 116:9423-9429.
- Cheatham, T. E., III, P. Cieplak, and P. A. Kollman. 1999. A modified version of the Cornell et al. force field with improved sugar pucker phases and helical repeat. *J. Biomol. Struct. Dynam.* 16:845-862.
- Cheatham, T. E., III, and P. A. Kollman. 1996. Observation of the A-DNA to B-DNA transition during unrestrained molecular dynamics in aqueous solution. *J. Mol. Biol.* 259:434-444.
- Cheatham, T. E., III, and P. A. Kollman. 1997. Molecular dynamics simulations highlight structural differences among DNA:DNA, RNA:RNA, and DNA:RNA hybrid duplexes. *J. Am. Chem. Soc.* 119:4805-4825.
- Cheatham, T. E., III, J. L. Miller, T. I. Spector, P. Cieplak, and P. A. Kollman. 1998. Molecular dynamics simulations on nucleic acid systems using the Cornell et al. force field and particle mesh Ewald electrostatics. *In Molecular Modeling of Nucleic Acids*. N. B. Leontis and J. SantaLucia, Jr., editors. American Chemical Society, Washington, DC. 285-303.
- Cieplak, P., T. E. Cheatham, III, and P. A. Kollman. 1997. Molecular dynamics simulations find that 3' phosphoramidate modified DNA duplexes undergo a B to A transition and normal DNA duplexes an A to B transition. *J. Am. Chem. Soc.* 119:6722-6730.
- Cornell, W. D., P. Cieplak, C. I. Bayly, I. R. Gould, K. M. Merz, Jr., D. M. Ferguson, D. C. Spellmeyer, T. Fox, J. W. Caldwell, and P. A. Kollman. 1995. A second generation force field for the simulation of proteins, nucleic acids, and organic molecules. *J. Am. Chem. Soc.* 117:5179-5197.
- Cowan, J. A., H.-W. Huang, and L.-Y. Hsu. 1993. Sequence selective coordination of  $\text{Mg}^{2+}(\text{aq})$  to DNA. *J. Inorg. Biochem.* 52:121-129.
- Darden, T., L. Perera, L. Li, and L. Pedersen. 1999. New tricks for modelers from the crystallography toolkit: the particle mesh Ewald algorithm and its use in nucleic acid simulations. *Structure.* 7:R55-R60.
- Dickerson, R. E. 1992. DNA Structure from A to Z. *Methods Enzymol.* 211:67-111.
- Dickerson, R. E., D. S. Goodsell, and S. Neidle. 1994. "... the tyranny of the lattice. ..." *Proc. Natl. Acad. Sci. USA.* 91:3579-3583.
- Duan, Y., P. Wilkosz, M. Crowley, and J. M. Rosenberg. 1997. Molecular dynamics simulation study of DNA dodecamer d(CGCGAATTCGCG) in solution: conformation and hydration. *J. Mol. Biol.* 272:553-572.
- El Hassan, M. A., and C. R. Calladine. 1997. Conformational characteristics of DNA: empirical classifications and a hypothesis for the conformational behaviour of dinucleotide steps. *Philos. Trans. R. Soc. Lond. A.* 355:43-100.
- Essmann, U., L. Perera, M. L. Berkowitz, T. Darden, H. Lee, and L. G. Pedersen. 1995. A smooth particle mesh Ewald method. *J. Chem. Phys.* 103:8577-8593.
- Gorin, A. A., V. B. Zhurkin, and W. K. Olson. 1995. B-DNA twisting correlates with base-pair morphology. *J. Mol. Biol.* 247:34-48.
- Hartmann, B., and R. Lavery. 1996. DNA structural forms. *Q. Rev. Biophys.* 29:309-368.
- Humphrey, W., A. Dalke, and K. Schulten. 1996. VMD—visual molecular dynamics. *J. Mol. Graph.* 14:33-38.
- Hunter, C. A. 1996. Sequence-dependent DNA structure. *BioEssays.* 18:157-162.
- Jayaram, B., and D. L. Beveridge. 1996. Modeling DNA in aqueous solutions: theoretical and computer simulation studies on the ion atmosphere of DNA. *Annu. Rev. Biophys. Biomol. Struct.* 25:367-394.
- Lavery, R. 1994. Modeling nucleic acids: fine structure, flexibility, and conformational transitions. *Adv. Comput. Biol.* 1:69-145.
- Lavery, R., and H. Sklenar. 1988. The definition of generalized helicoidal parameters and of axis curvature for irregular nucleic acids. *J. Biomol. Struct. Dyn.* 6:63-91.
- Lee, H., T. Darden, and L. Pedersen. 1995a. Accurate crystal molecular dynamics simulations using particle-mesh-Ewald: RNA dinucleotides—ApU and GpC. *Chem. Phys. Lett.* 243:229-235.
- Lee, H., T. A. Darden, and L. G. Pedersen. 1995b. Molecular dynamics simulation studies on a high-resolution Z-DNA crystal. *J. Chem. Phys.* 102:3830-3834.
- MacKerrell, A. D., Jr. 1997. Influence of magnesium ions on duplex DNA structural, dynamic, and solvation properties. *J. Phys. Chem. B.* 101:646-650.
- Nelson, H. C. M., J. T. Finch, B. F. Luisi, and A. Klug. 1987. The structure of an oligo(dA)-oligo(dT) tract and its biological implications. *Nature (Lond.)*. 330:221-226.
- Pearlman, D. A., D. A. Case, J. W. Caldwell, W. S. Ross, T. E. Cheatham, III, D. M. Ferguson, G. L. Seibel, U. C. Singh, P. K. Weiner, and P. A. Kollman. 1995. AMBER4.1. University of California, San Francisco.
- Porschke, D. 1978. The mode of  $\text{Mg}^{++}$  binding to oligonucleotides. Inner sphere complexes as markers for recognition? *Nucleic Acids Res.* 6:883-898.



- Prive, G. G., K. Yanagi, and R. E. Dickerson. 1991. Structure of the B-DNA decamer C-C-A-A-C-G-T-T-G-G and comparison with isomorphous decamers C-C-A-A-G-A-T-T-G-G and C-C-A-G-G-C-C-T-G-G. *J. Mol. Biol.* 217:177–199.
- Ramakrishnan, B., and M. Sundaralingam. 1993. Crystal packing effects on A-DNA helix parameters—a comparative study of the isoforms of the tetragonal and hexagonal family of octamers with differing base sequences. *J. Biomol. Struct. Dyn.* 11:11–26.
- Saenger, W. 1984. Principles of Nucleic Acid Structure. Springer-Verlag, New York.
- Sarma, R. H., M. H. Sarma, L. Dai, and K. Umemoto. 1997. GC rich DNA oligonucleotides with narrow minor groove width. *FEBS Lett.* 418:76–82.
- Sheeler, P., and D. E. Bianchi. 1980. Cell Biology: Structure, Biochemistry, and Function. John Wiley and Sons, New York.
- Shui, X., L. McFail-Isom, G. G. Hu, and L. D. Williams. 1998a. The B-DNA dodecamer at high resolution reveals a spine of water on sodium. *Biochemistry.* 37:8341–8355.
- Shui, X., C. C. Sines, L. McFail-Isom, D. VanDerveer, and L. D. Williams. 1998b. Structure of the potassium form of CGCGAATTCGCG: DNA deformation by electrostatic collapse around inorganic cations. *Biochemistry.* 37:16877–16887.
- Swaminathan, S., G. Ravishanker, and D. L. Beveridge. 1991. Dynamics of B-DNA including counterions and water: a 140 psec trajectory for d(CGCGAATTCGCG) based on the GROMOS force field. *J. Am. Chem. Soc.* 113:5027–5040.
- Tereshko, V., G. Minasov, and M. Egli. 1999. The Dickerson-Drew B-DNA dodecamer revisited at atomic resolution. *J. Am. Chem. Soc.* 121:470–471.
- Tippin, D. B., and M. Sundaralingam. 1997. Comparison of major groove hydration in isomorphous A-DNA octamers and dependence on base sequence and local helix geometry. *Biochemistry.* 36:536–543.
- Westhof, E., C. Rubin-Carrez, and V. Fritsch. 1995. The use of molecular dynamics simulations for modelling nucleic acids. In Computer Modelling in Molecular Biology. J. M. Goodfellow, editor. VCH, New York. 103–131.
- Xu, X.-P., W.-L. A. K. Chiu, and S. C. F. Au-Yeung. 1998. Chemical shift and structure relationship in nucleic acids: correlation of backbone torsion angles  $\gamma$  and  $\alpha$  with  $^{13}\text{C}$  chemical shifts. *J. Am. Chem. Soc.* 120:4230–4231.
- York, D. M., T. A. Darden, and L. G. Pedersen. 1993. The effect of long-range electrostatic interactions in simulations of macromolecular crystals: a comparison of the Ewald and truncated list methods. *J. Chem. Phys.* 99:8345–8348.
- York, D. M., A. Wlodawer, L. G. Pedersen, and T. A. Darden. 1994. Atomic-level accuracy in simulations of large protein crystals. *Proc. Natl. Acad. Sci. USA.* 91:8715–8718.
- York, D. M., W. Yang, H. Lee, T. Darden, and L. G. Pedersen. 1995. Toward the accurate modeling of DNA: the importance of long-range electrostatics. *J. Am. Chem. Soc.* 117:5001–5002.
- Young, M. A., B. Jayaram, and D. L. Beveridge. 1997a. Intrusion of counterions into the spine of hydration in the minor groove of B-DNA: fractional occupancy of electronegative pockets. *J. Am. Chem. Soc.* 119:59–69.
- Young, M. A., G. Ravishanker, and D. L. Beveridge. 1997b. A 5-nano-second molecular dynamics trajectory for B-DNA: analysis of structure, motions, and solvation. *Biophys. J.* 73:2313–2336.